

# Quantum defects of Rydberg excitons in cuprous oxide: A semiclassical spherical model

Jan Ertl<sup>1</sup>, Patric Rommel<sup>1</sup>, Jörg Main<sup>1\*</sup>

<sup>1</sup>Institut für Theoretische Physik I, Universität Stuttgart, 70550 Stuttgart, Germany.

\*Corresponding author(s). E-mail(s): [main@itp1.uni-stuttgart.de](mailto:main@itp1.uni-stuttgart.de);

## Abstract

Excitons, i.e. the bound states of an electron and a positively charged hole are the solid state analogue of the hydrogen atom. As such they exhibit a Rydberg series, which in cuprous oxide has been observed up to high principal quantum numbers by T. Kazimierczuk et al. [Nature 514, 343 (2014)]. In this energy regime the quantum mechanical properties of the system can be understood in terms of classical orbits by the application of semiclassical techniques. In fact the first theoretical explanation of the spectrum of the hydrogen atom within Bohr's atomic model was a semiclassical one using classical orbits and a quantization condition for the angular momentum. Contrary to the hydrogen atom, the degeneracy of states with the same principal quantum number  $n$  is lifted in exciton spectra. This is similar to the situation in alkali atoms, where these splittings are caused by the interaction of the excited electron with the ionic core. For excitons in cuprous oxide, these splittings occur due to the influence of the complex band structure of the crystal. Using an adiabatic approach and analytically derived energy surfaces, we develop a semiclassical spherical model and determine, via semiclassical torus quantization, the quantum defects of various angular momentum states.

## 1 Introduction

At the end of the 19th century it became evident that classical physics must be extended to describe phenomena observed in microscopic systems, such as the distinct lines of atomic spectra, where the energy is quantized. The first quantitative

description was introduced by Balmer in 1885 providing a formula correctly reproducing the lines in the range of visible light for the hydrogen atom [1]. This formula was extended by Rydberg [2] predicting the existence of other series in addition to the Balmer series which only includes transitions from or to states with principal quantum number  $n = 2$ . The Rydberg formula was confirmed after the Lyman series [3] ( $n = 1$ ) and the Paschen series [4] ( $n = 3$ ) were found. The first theoretical explanation for the hydrogenic spectra was given by Bohr [5] by postulating that the electron can only move on certain classical orbits fulfilling a quantization condition for the angular momentum, which allows for a derivation of the empirically known Rydberg formula. Sommerfeld extended the quantization of only circular orbits to ellipses via a quantization condition and quantum numbers for all three spherical coordinates [6].

The work by Bohr and Sommerfeld preceded the modern formulation of quantum mechanics where the particles are described by a wave function. A semiclassical treatment of the wave functions reveals that one also has to account for the caustics when performing a semiclassical torus quantization. To this aim one has to consider the Maslov index counting the number of reflections and turning points along independent paths on the torus. The resulting Einstein-Brillouin-Keller (EBK) quantization condition [7–10] for the corresponding action variables provides good results for a wide range of integrable and even near-integrable systems. However, as already noticed by Einstein [7] the EBK quantization cannot be applied to non-integrable or chaotic systems. Semiclassical theories for such systems have been derived in the 1970's by Gutzwiller [11–14].

The hydrogen-like model is also appropriate to deal with non-hydrogenic atoms with one highly excited electron. For these Rydberg atoms the distance of the electron to the nucleus and the other electrons is large, meaning that the ionic core can approximately be treated as one entity with net charge  $+e$ . For the hydrogen atom all states with a given principal quantum number  $n$  are degenerate. For non-hydrogenic atoms this degeneracy is partly lifted. In the classical picture this can be understood when looking at the corresponding orbits. For states with low angular momentum quantum numbers  $l$  the orbits of the excited electron come closer to the core, which in this region is no longer fully screened by the other electrons. Thus, the excited electron experiences a stronger Coulomb interaction, lowering the binding energy. To capture these deviations from the hydrogen spectrum, Rydberg himself introduced a correction scheme to modify the expressions for the wave number by subtracting a non-integer quantum defect  $\delta_{n,l}$  from the principal quantum number and substituting  $n$  by  $n^* = n - \delta_{n,l}$  in the Rydberg formula [2]. As the screening of the core becomes stronger for increasing angular momentum quantum number, the quantum defects typically decrease with increasing  $l$ .

Excitons consisting of a positively charged hole and a negatively charged electron are the solid-state analogue of the hydrogen atom. For most systems only the lowest principal quantum numbers are experimentally accessible [15–17]. This was also true for first experiments on cuprous oxide [18], however, this has changed since the observation of high Rydberg excitons with principal quantum numbers up to  $n = 25$  in the seminal work by Kazimierczuk et al. [19]. Nowadays, a Rydberg series of  $p$  states can be traced up to  $n = 30$  [20]. The rough features of the spectra can be explained

within a simple hydrogen-like model by the Coulomb interaction between electron and hole, however, a detailed description requires the consideration of band-structure effects of the crystal [21–23], which cause the reduction of the spherical symmetry to the cubic point group  $O_h$  [24]. Additional central-cell corrections become important when electron and hole come close to each other [25]. In the 1950’s, Hermann Haken provided fundamental contributions to this topic, including the Haken-potential [26–31]. Later, he founded the field of synergetics dealing with complex systems. Here, microscopic degrees of freedom are adiabatically eliminated, allowing for a description of the system in terms of a small number of order parameters. We have tried to bridge the two topics by utilizing an adiabatic approach to the spin degrees of freedom in the exciton dynamics [32]. This leads to a classical description of the nonlinear exciton dynamics via energy surfaces in momentum space and the observation of a transition from a regular to chaotic motion [33]. The classical periodic orbits have been linked to the quantum spectra of the system by application of semiclassical techniques [34, 35]. A review on experimental and theoretical results on the yellow exciton series in cuprous oxide is given in a recent article by Heckötter et al. [36]. The highly excited  $p$  states of the yellow exciton series can be described by a Rydberg formula with quantum defects [19]. This concept can also be applied to other angular momentum states [37, 38]. Uihlein et al. [39] adjusted a spherical model to experimental spectra.

Our goal in this article is to derive quantum defects of the yellow exciton series from a semiclassical spherical model. We start, in Sec. 2.1, from the full model including the cubic contributions and apply, in Sec. 2.2, an adiabatic approach to obtain energy surfaces for a classical description of the exciton dynamics. Analytical formulas for these energy surfaces are derived in Sec. 2.3. In Sec. 3.1 we obtain spherically symmetric energy surfaces using numerical and analytical methods, which are the basis for the semiclassical EBK quantization in Sec. 3.2. Considering the probability distribution of the exciton in momentum space leads to order parameters describing the different angular momentum manifolds. A conclusion and outlook are given in Sec. 4.

## 2 Theory

Excitons in a semiconductor are formed when an electron is excited from the valence band into the conduction band. Instead of taking into account the interaction of the excited electron with the solid and all its constituents, one treats the missing hole in the valence band as positively charged quasi particle, which can, via the Coulomb interaction with the electron, form a hydrogen-like bound state, the exciton.

### 2.1 Hamiltonian for excitons in cuprous oxide

The Hamiltonian for a theoretical description of excitons is given as

$$H = H_e(\mathbf{p}_e) + H_h(\mathbf{p}_h) - \frac{e^2}{4\pi\epsilon_0\epsilon} \frac{1}{|\mathbf{r}_e - \mathbf{r}_h|}, \quad (1)$$

with the kinetic energy of the electron  $H_e(\mathbf{p}_e)$  and the kinetic energy of the hole  $H_h(\mathbf{p}_h)$ . The Coulomb interaction is screened by the permittivity  $\epsilon$  due to the crystal

environment. In cuprous oxide the kinetic energy for the hole follows a parabolic dispersion [23, 37, 38]

$$H_e(\mathbf{p}_e) = E_g + \frac{\mathbf{p}_e^2}{2m_e}, \quad (2)$$

with the gap energy  $E_g$  and the effective electron mass  $m_e$ . The kinetic energy of the hole is more complicated, because the uppermost valence band has a threefold degeneracy at the  $\Gamma$  point. This situation can be modeled by introducing a quasispin  $I = 1$ . Due to the spin-orbit coupling of the hole spin  $S_h = 1/2$  and the quasispin

$$H_{so} = \frac{2}{3}\Delta \left( 1 + \frac{1}{\hbar^2} \mathbf{I} \cdot \mathbf{S}_h \right), \quad (3)$$

the valence band splits, leading to a yellow series and a green series with heavy holes (hh) and light holes (lh). The Hamiltonian for the hole in the valence band needs to consider all terms including momenta, quasispin and hole spin in line with the cubic  $O_h$  symmetry of the crystal. Up to second order of the momenta the Hamiltonian for the hole reads [22, 23, 37, 38, 40]

$$\begin{aligned} H_h(\mathbf{p}) = & H_{so} + (1/2\hbar^2 m_0) \{ \hbar^2 (\gamma_1 + 4\gamma_2) \mathbf{p}^2 + 2(\eta_1 + 2\eta_2) \mathbf{p}^2 (\mathbf{I} \cdot \mathbf{S}_h) \\ & - 6\gamma_2 (p_1^2 \mathbf{I}_1^2 + \text{c.p.}) - 12\eta_2 (p_1^2 \mathbf{I}_1 \mathbf{S}_{h1} + \text{c.p.}) \\ & - 12\gamma_3 (\{p_1, p_2\} \{ \mathbf{I}_1, \mathbf{I}_2 \} + \text{c.p.}) \\ & - 12\eta_3 (\{p_1, p_2\} (\mathbf{I}_1 \mathbf{S}_{h2} + \mathbf{I}_2 \mathbf{S}_{h1}) + \text{c.p.}) \}, \end{aligned} \quad (4)$$

with the Luttinger parameters  $\gamma_i, \eta_i$ . While in principle higher orders of the momenta are possible, their contributions can be neglected for our purposes [25]. In our classical and semiclassical approach we also ignore central-cell corrections, which affect the even-parity excitons [25]. Using relative and center-of-mass coordinates and neglecting the center-of-mass motion, the full Hamiltonian for excitons in cuprous oxide reads

$$\begin{aligned} H = & E_g + H_{so} + (1/2\hbar^2 m_0) \{ \hbar^2 (\gamma'_1 + 4\gamma_2) \mathbf{p}^2 + 2(\eta_1 + 2\eta_2) \mathbf{p}^2 (\mathbf{I} \cdot \mathbf{S}_h) \\ & - 6\gamma_2 (p_1^2 \mathbf{I}_1^2 + \text{c.p.}) - 12\eta_2 (p_1^2 \mathbf{I}_1 \mathbf{S}_{h1} + \text{c.p.}) - 12\gamma_3 (\{p_1, p_2\} \{ \mathbf{I}_1, \mathbf{I}_2 \} + \text{c.p.}) \\ & - 12\eta_3 (\{p_1, p_2\} (\mathbf{I}_1 \mathbf{S}_{h2} + \mathbf{I}_2 \mathbf{S}_{h1}) + \text{c.p.}) \} - \frac{e^2}{4\pi\epsilon_0\epsilon} \frac{1}{|\mathbf{r}_e - \mathbf{r}_h|}, \end{aligned} \quad (5)$$

with  $\gamma'_1 = \gamma_1 + m_0/m_e$ . The Hamiltonian (5) can be split into terms with spherical symmetry and terms with reduced cubic symmetry by using irreducible tensors [23, 41–43],

$$\begin{aligned} H = & E_g - \frac{e^2}{4\pi\epsilon_0\epsilon} \frac{1}{r} + \frac{2}{3}\Delta \left( 1 + \frac{1}{\hbar^2} I^{(1)} \cdot S_h^{(1)} \right) + \frac{\gamma'_1}{2\hbar^2 m_0} \left[ \hbar^2 p^2 - \frac{\mu'}{3} P^{(2)} \cdot I^{(2)} \right. \\ & \left. + \frac{\delta'}{3} \left( \sum_{k=\pm 4} [P^{(2)} \times I^{(2)}]_k^{(4)} + \frac{\sqrt{70}}{5} [P^{(2)} \times I^{(2)}]_0^{(4)} \right) \right] + \frac{3\eta_1}{\hbar^2 m_0} \left[ \frac{1}{3} p^2 (I^{(1)} \cdot S_h^{(1)}) \right] \end{aligned}$$

$$-\frac{\nu}{3} P^{(2)} \cdot D^{(2)} + \frac{\tau}{3} \left( \sum_{k=\pm 4} [P^{(2)} \times D^{(2)}]_k^{(4)} + \frac{\sqrt{70}}{5} [P^{(2)} \times D^{(2)}]_0^{(4)} \right). \quad (6)$$

For the tensor operators we use the same convention as in Refs. [23, 43]. The coefficients

$$\mu' = \frac{6\gamma_3 + 4\gamma_2}{5\gamma_1'} = 0.0586, \quad \nu = \frac{6\eta_3 + 4\eta_2}{5\eta_1} = 2.167 \quad (7)$$

give the strength of the spherical contributions, whereas the strength of the cubic contributions is characterized by

$$\delta' = \frac{\gamma_3 - \gamma_2}{\gamma_1'} = -0.404, \quad \tau = \frac{\eta_3 - \eta_2}{\eta_1} = 1.500. \quad (8)$$

For the calculation of quantum defects in Sec. 3 we use a spherical model, however, contributions of the cubic terms in Eq. (6) will be considered in a semiclassical picture by averaging the energy surfaces, derived in Sec. 2.3, over the spherical angle coordinates.

## 2.2 Adiabatic approach to the exciton dynamics

In this article we use a semiclassical picture to compute the quantum defects of Rydberg excitons in cuprous oxide. For the classical exciton dynamics we resort to the adiabatic approach presented in Ref. [32]. The basic idea is that for Rydberg excitons with principal quantum numbers  $n \gtrsim 3$  the energy spacing between adjacent Rydberg levels is small compared to the spacings caused by the spin-orbit coupling, and thus the exciton dynamics in the coordinate and momentum space is much slower than the spin dynamics. In analogy to the Born-Oppenheimer approximation for molecules, this allows for a classical or semiclassical treatment of the exciton dynamics, where the coordinate and momentum operators in the Hamiltonian (5) are replaced by classical variables and only the spin degrees of freedom are considered quantum mechanically. The energy surfaces are obtained by diagonalizing the Hamiltonian  $H_{\text{band}}$  defined by the Hamiltonian in Eq. (6) excluding the gap energy  $E_g$ , the term  $\gamma_1' \mathbf{p}^2 / (2m_0)$ , and the Coulomb potential, for given values of the classical momenta  $\mathbf{p}$  in the basis  $|m_I, m_{S_h}\rangle$  for the quasispin and hole spin degrees of freedom, with  $m_I = 0, \pm 1$  and  $m_{S_h} = \pm 1/2$ . This yields a  $(6 \times 6)$ -dimensional eigenvalue problem

$$\mathbf{H}_{\text{band}}(\mathbf{p})\mathbf{c} = W_k(\mathbf{p})\mathbf{c} \quad (9)$$

for energy surfaces  $W_k(\mathbf{p})$ . In general, the eigenvalues of a  $6 \times 6$  matrix cannot be found analytically, however, solutions can be obtained numerically, e.g., by using an appropriate *LAPACK* routine [44]. It should be noted that the eigenvalues of the eigenvalue problem (9) are twofold degenerate, i.e., there are only three independent energy surfaces, where the lowest one belongs to the yellow exciton series and the two upper surfaces are related to the green series with heavy and light hole. This is due to the Kramers degeneracy in time-reversal symmetric systems with a half-integer total

spin [45]. The calculation of the energy surfaces by numerical diagonalizations of the  $6 \times 6$  matrices is rather time-consuming. Furthermore, for the computation of classical exciton orbits by solving Hamilton's equations of motion and their stability analysis first and second derivatives of the energy surfaces  $W_k(\mathbf{p})$  are required. In addition, the energy surfaces are equivalent to the electronic band structure. Therefore, analytical expressions for the energy surfaces are highly desirable [46]. Indeed, as will be shown below, it is possible to exploit Kramers' degeneracy to find analytical expressions for the energy surfaces.

### 2.3 Analytical expressions for the energy surfaces

The starting point for the derivation of analytical expressions for the energy surfaces is the characteristic polynomial of the  $6 \times 6$  matrix in Eq. (9), which takes the form

$$\chi(\lambda) = \lambda^6 + c_5\lambda^5 + c_4\lambda^4 + c_3\lambda^3 + c_2\lambda^2 + c_1\lambda + c_0. \quad (10)$$

In general, there are no analytical formulas for the roots of a polynomial of degree five or higher. However, for the special case of excitons in cuprous oxide analytical expressions can be obtained by exploiting Kramers' degeneracy. Since every energy surface is twofold degenerate, the characteristic polynomial (10) can be expressed as

$$[W_y(\mathbf{p}) - \lambda]^2 [W_{g,hh}(\mathbf{p}) - \lambda]^2 [W_{g,lh}(\mathbf{p}) - \lambda]^2 = 0. \quad (11)$$

By comparing the left hand side of Eq. (11) with Eq. (10) and using the abbreviations  $W_3 = W_y(\mathbf{p})$ ,  $W_2 = W_{g,hh}(\mathbf{p})$ , and  $W_1 = W_{g,lh}(\mathbf{p})$  the following system of equations for the energy surfaces is obtained:

$$c_5 = -2(W_1 + W_2 + W_3), \quad (12a)$$

$$c_4 = (W_1 + W_2 + W_3)^2 + 2W_1W_2 + 2W_1W_3 + 2W_2W_3, \quad (12b)$$

$$c_3 = -2(W_1^2W_2 + W_1^2W_3 + W_1W_2^2 + W_1W_3^2 + W_2^2W_3 + W_2W_3^2 + 4W_1W_2W_3), \quad (12c)$$

$$c_2 = W_1^2W_2^2 + W_1^2W_3^2 + W_2^2W_3^2 + 4(W_1^2W_2W_3 + W_1W_2^2W_3 + W_1W_2W_3^2), \quad (12d)$$

$$c_1 = -2(W_1^2W_2^2W_3 + W_1^2W_2W_3^2 + W_1W_2^2W_3^2), \quad (12e)$$

$$c_0 = W_1^2W_2^2W_3^2. \quad (12f)$$

Since there are six equations for three potential surfaces, this system is overdetermined. However, these equations are not independent. To obtain a solution for the energy surfaces it is therefore sufficient to consider the first three equations (12a)–(12c). Using these expressions one arrives at a polynomial of degree three for the energy surfaces that needs to vanish,

$$W_k^3 + \frac{c_5}{2}W_k^2 + \frac{4c_4 - c_5^2}{8}W_k + \frac{8c_3 - 4c_4c_5 + c_5^3}{16} = 0. \quad (13)$$

The solutions of Eq. (13) can be found by applying Cardano's formula, which for real-valued solutions takes the form [47]

$$W_k = -\frac{c_5}{6} + \sqrt{-\frac{4p_c}{3}} \cos \left[ \frac{1}{3} \arccos \left( -\frac{q_c}{2} \sqrt{-\frac{27}{p_c^3}} \right) - \frac{2\pi(k-1)}{3} \right], \quad (14)$$

where  $p_c$  and  $q_c$  are given by the coefficients of the characteristic polynomial  $c_i$ , i.e.

$$p_c = \frac{c_4}{2} - \frac{5c_5^2}{24}, \quad q_c = \frac{c_3}{2} - \frac{c_4c_5}{3} + \frac{5c_5^3}{54}. \quad (15)$$

To evaluate the energy surfaces in Eq. (14) we need to insert the expressions for  $c_5$ ,  $p_c$ , and  $q_c$  in terms of the momenta  $\mathbf{p}$  and the material parameters of cuprous oxide. The following expressions are obtained:

$$c_5 = -4\Delta, \quad (16a)$$

$$p_c = a_0 + a_1(p_1^2 + p_2^2 + p_3^2) + a_2(p_1^2 + p_2^2 + p_3^2)^2 + a_3(p_1^2p_2^2 + p_1^2p_3^2 + p_2^2p_3^2), \quad (16b)$$

$$q_c = b_0 + b_1(p_1^2 + p_2^2 + p_3^2) + b_2(p_1^2 + p_2^2 + p_3^2)^2 + b_3(p_1^2 + p_2^2 + p_3^2)^3 \\ + b_4(p_1^2p_2^2 + p_1^2p_3^2 + p_2^2p_3^2) + b_5(p_1^2 + p_2^2 + p_3^2)(p_1^2p_2^2 + p_1^2p_3^2 + p_2^2p_3^2) \\ + b_6(p_1^2p_2^2p_3^2), \quad (16c)$$

with the constant coefficients

$$a_0 = -\frac{\Delta^2}{3}, \quad (17a)$$

$$a_1 = -\frac{\Delta\eta_1}{m_0}, \quad (17b)$$

$$a_2 = -\frac{3}{100m_0^2} \left\{ \gamma_1'^2 (6\delta' - 5\mu')^2 + \eta_1^2 [25 + 2(5\nu - 6\tau)^2] \right\}, \quad (17c)$$

$$a_3 = \frac{9}{5m_0^2} [\gamma_1'^2 (\delta'^2 - 5\delta'\mu') + 2\eta_1^2 \tau (-5\nu + \tau)], \quad (17d)$$

and

$$b_0 = \frac{2\Delta^3}{27}, \quad (18a)$$

$$b_1 = \frac{\Delta^2\eta_1}{3m_0}, \quad (18b)$$

$$b_2 = \frac{\Delta\eta_1}{50m_0^2} [2\gamma_1' (6\delta' - 5\mu')(5\nu - 6\tau) - \eta_1(-5 + 5\nu - 6\tau)(5 + 5\nu - 6\tau)], \quad (18c)$$

$$b_3 = \frac{1}{500m_0^3} [\gamma_1'^3 (6\delta' - 5\mu')^3 - 3\eta_1^2 \gamma_1' (6\delta' - 5\mu')(-10 + 5\nu - 6\tau)(5\nu - 6\tau) \\ - \eta_1^3 (-5 + 10\nu - 12\tau)(5 + 5\nu - 6\tau)^2], \quad (18d)$$

$$b_4 = -\frac{6\Delta\eta_1}{5m_0^2} [\delta'\gamma_1'(5\nu - 2\tau) + \tau(5\gamma_1'\mu' + 5\eta_1\nu - \eta_1\tau)], \quad (18e)$$

$$b_5 = \frac{9}{50m_0^3} \left\{ -6\delta'^3\gamma_1'^3 + 35\delta'^2\gamma_1'^3\mu' \right. \\ \left. - \eta_1^2\tau [2\eta_1(5 + 5\nu - 6\tau)(5\nu - \tau) + 5\gamma_1'\mu'(10 - 10\nu + 7\tau)] \right. \\ \left. + \delta'\gamma_1' [-25\gamma_1'^2\mu'^2 + \eta_1^2(25(-2 + \nu)\nu + 10(2 - 7\nu)\tau + 18\tau^2)] \right\}, \quad (18f)$$

$$b_6 = -\frac{27}{10m_0^3} (\delta'\gamma_1' - \eta_1\tau) [2\delta'^2\gamma_1'^2 + \eta_1\tau(15\gamma_1'\mu' - 30\eta_1\nu - 4\eta_1\tau) \\ + \delta'\gamma_1'(15\gamma_1'\mu' + 2\eta_1\tau)]. \quad (18g)$$

We finally obtain the Hamiltonian

$$H = E_g + \frac{\gamma_1'}{2m_0} \mathbf{p}^2 - \frac{e^2}{4\pi\epsilon_0\epsilon} \frac{1}{r} + W_k(\mathbf{p}) \quad (19)$$

for a classical description of the exciton dynamics via three distinct analytically given energy surfaces  $W_k(\mathbf{p})$  in momentum space. To investigate the yellow exciton series we can now choose the lowest energy surface  $W_y(\mathbf{p})$  and integrate Hamilton's equations of motion

$$\dot{r}_i = \frac{\gamma_1'}{m_0} p_i + \frac{\partial W_y(\mathbf{p})}{\partial p_i}, \quad \dot{p}_i = -\frac{e^2}{4\pi\epsilon_0\epsilon} \frac{r_i}{|\mathbf{r}|^3}. \quad (20)$$

For our calculations we use exciton-Hartree units obtained by setting  $\hbar = e = m_0/\gamma_1' = 1/(4\pi\epsilon_0\epsilon) = 1$ , and the material parameters of cuprous oxide as given in Eqs. (7) and (8).

### 3 Results and discussion

The energy surfaces  $W_k(\mathbf{p})$  in Eq. (14) incorporate the complex band structure of the system and thus model the complex interaction of the exciton with the other electrons of the solid. Considering the reduced  $O_h$  symmetry of the system the exciton dynamics described by the equations of motion (20) exhibits a mostly regular dynamics on tori for the yellow exciton series and a strong transition to chaotic dynamics for the green exciton series [33, 35]. Here, our goal is to obtain the quantum defects of the yellow excitons in cuprous oxide. While a hydrogen-like model due to the high  $O(4)$  symmetry of the Coulomb problem is not capable of producing a splitting of the different  $l$  states, this can be achieved using a model with spherical symmetry. To this aim, in a first first step, we derive spherically symmetric energy surfaces, which are then used, in a second step, for semiclassical EBK quantization.

#### 3.1 Spherically symmetric energy surfaces

The energy surface  $W_y(\mathbf{p})$  for the yellow exciton series in Eq. (14) has cubic symmetry  $O_h$ , i.e., the energies depend on the orientation of the momentum. One possibility to obtain spherically symmetric energy surfaces is to neglect the terms with cubic



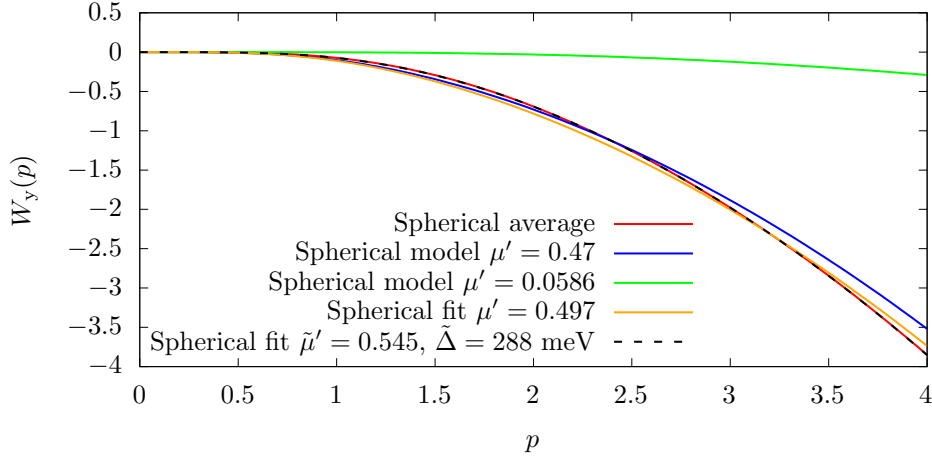


**Fig. 1** Comparison of the spherical average  $\overline{W}_y(p)$  in Eq. (23) (red line) with the spherical model  $\widetilde{W}_y(p)$  in Eq. (21) using  $\mu' = 0.0586$  (green line) and  $\mu' = 0.47$  (blue line). A fit of the spherical model to the spherical average yields  $\mu' = 0.497$  (orange line). The spin-orbit splitting is fixed to the experimental value  $\Delta = 131$  meV except for the black dashed line where nearly perfect agreement with the spherical average is obtained when  $\tilde{\Delta} = 288$  meV and  $\tilde{\mu}' = 0.545$  are used as fit parameters for  $\Delta$  and  $\mu'$  in Eq. (21).

symmetry in the Hamiltonian (6) and thus to set  $\nu = \delta' = \tau = \eta_1 = 0$  in Eq. (14). In this case the coefficients  $a_3$ ,  $b_4$ ,  $b_5$ , and  $b_6$  in Eqs. (16)–(18) vanish. The remaining non-zero coefficients belong to powers of  $\mathbf{p}^2$  and thus makes the energy surface  $W_y(p)$  spherically symmetric. In this special case Eq. (14) can be further simplified to

$$\widetilde{W}_y(p) = \frac{1}{4} \left( 2\Delta + \frac{\mu' \gamma_1'}{m_0} p^2 - \sqrt{4\Delta^2 + 4\Delta \frac{\mu' \gamma_1'}{m_0} p^2 + 9 \frac{\mu'^2 \gamma_1'^2}{m_0^2} p^4} \right). \quad (21)$$

Using exciton-Hartree units with  $\gamma_1'/m_0 = 1$ , Eq. (21) only depends on the spin-orbit splitting  $\Delta = 131$  meV and the material parameter  $\mu' = 0.0586$  describing the strength of band structure contributions. The obtained energy surface  $\widetilde{W}_y(p)$  for these parameters is shown as the green line in Fig. 1. The chosen momentum range  $0 \leq p \leq 4$  is obtained from the semiclassical quantization condition for the angular momentum  $L = \hbar(l + \frac{1}{2})$ , i.e., we can estimate that the maximum momentum for a given  $l$  in a Rydberg state is given by

$$p_{\max} = \frac{4}{2l + 1}, \quad (22)$$

which yields  $p_{\max} = 4$  for  $s$  states.

The complete neglect of all terms with cubic symmetry may not be justified and thus may not lead to quantitatively reasonable results. A more reliable approach is obtained by a spherical average of the energy surfaces in Eq. (14) over all orientations

of the momenta, i.e.,

$$\overline{W}_y(p) = \frac{1}{4\pi} \int_0^{2\pi} \int_0^\pi W_y(p, \varphi_p, \vartheta_p) d\Omega. \quad (23)$$

For the computation of the integrals we use an efficient spherical design [48]. Note that due to the  $O_h$  symmetry of the energy surfaces the full  $\Omega$  space consists of 48 fundamental regions, which are related by symmetry properties, and thus in principle the average over a reduced fundamental area  $\Omega_f = 4\pi/48$  would be sufficient. The energy surface  $\overline{W}_y(p)$  obtained from Eq. (23) is shown by the red line in Fig. 1. Evidently, the green and red energy surfaces do not coincide, which illustrates that ignoring of the cubic terms is indeed not justified. However, when using  $\Delta$  and  $\mu'$  in Eq. (21) as free parameters, the analytical form of the spherically symmetric energy surface  $\widetilde{W}_y(p)$  can be adjusted to the numerical surface  $\overline{W}_y(p)$  in Eq. (23). With the obtained fit parameters  $\widetilde{\Delta} = 288$  meV and  $\widetilde{\mu}' = 0.545$  the corresponding dashed black line in Fig. 1 nearly perfectly coincides with the red line for the numerical surface  $\overline{W}_y(p)$ . When taking for  $\Delta$  the true value of the spin-orbit coupling and only using  $\mu'$  as a fit parameter, we obtain  $\mu' = 0.497$ , see the orange line in Fig. 1. The agreement with the red line is less perfect but still reasonable when only using a single fit parameter. It is interesting to note that  $\mu' = 0.497$  is close to the value of  $\mu' = 0.47$  (see the blue line in Fig. 1), obtained in Ref. [39] when fitting a spherically symmetric Hamiltonian to experimental spectra. This is a remarkable result, the small deviations of the two fit parameters may be due to the usage of slightly different material parameters. The analytical functions  $\widetilde{W}_y(p)$  in Eq. (21), adjusted to the spherically symmetric energy surfaces  $\overline{W}_y(p)$  given in Eq. (23), are the basis for the computation of quantum defects via semiclassical EBK quantization in the following section 3.2.

### 3.2 Semiclassical EBK quantization

In the spherically symmetric case the action angle variables are characterized by spherical coordinates and a semiclassical quantization can be obtained using the EBK quantization conditions [7–9]

$$J_\varphi = \frac{1}{2\pi} \oint L_z d\varphi = m, \quad (24a)$$

$$J_\vartheta = \frac{1}{2\pi} \oint \sqrt{\mathbf{L}^2 - \frac{L_z^2}{\sin^2 \vartheta}} d\vartheta = l - |m| + \frac{1}{2}, \quad (24b)$$

$$J_r = \frac{1}{2\pi} \oint p_r dr = n_r + \frac{1}{2}, \quad (24c)$$

where the first two equations describe the quantization of the angular momentum vector  $\mathbf{L}$  with angular and magnetic quantum numbers  $l$  and  $m$ . The radial momentum  $p_r(E, r; l)$  in the third equation depends on the energy surface  $\widetilde{W}_y(p)$ , the angular momentum  $\mathbf{L}$ , and the energy  $E$ , and is obtained by a numerical root search of the

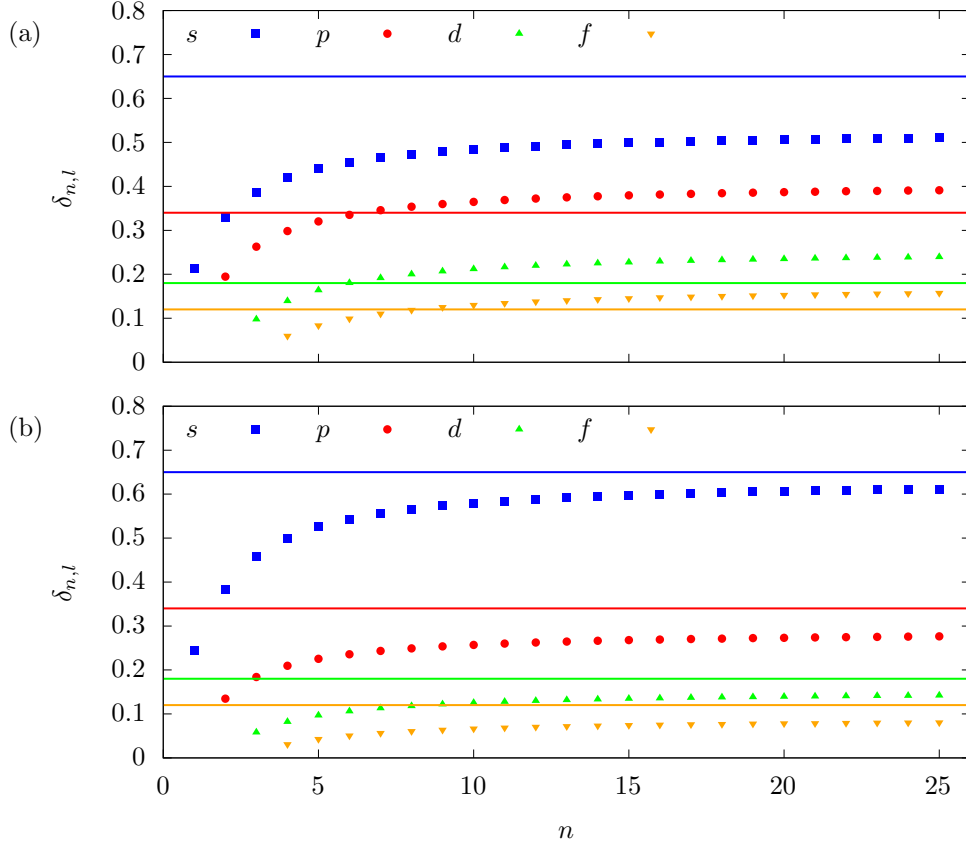


**Fig. 2** (a) Quantum defects  $\delta_{n,l}$  for  $s$ ,  $p$ ,  $d$ , and  $f$  states obtained with the spherically symmetric energy surfaces  $\widetilde{W}_y(p)$  with parameters  $\Delta = 131$  meV and  $\mu' = 0.47$ . (b) Improved quantum defects  $\delta_{n,l}$  obtained from a spherical model using values  $\mu'_l$  optimized for different  $l$  manifolds. Here,  $\mu'_l$  acts as an order parameter characterizing the strength of the band structure in the various  $l$  manifolds. The solid lines mark the quantum defects in the limit of large principal quantum numbers  $n$  given in Ref. [49].

equation

$$E = E_g + \frac{1}{2\mu} (p_r^2 + \hbar^2(l + 1/2)^2/r^2) + \widetilde{W}_y \left( p = \sqrt{p_r^2 + \hbar^2(l + 1/2)^2/r^2} \right) - \frac{1}{r}. \quad (25)$$

The l.h.s. of the quantization condition (24c) is evaluated by numerical integration of  $p_r = p_r(E, r; l)$  between the classical turning points  $r_{\min}$  and  $r_{\max}$ . The quantized energies  $E_{n,l}$  are finally determined, for a given radial quantum number  $n_r = n - l - 1$ , from Eq. (24c) via numerical root search. The energy eigenvalues  $E_{n,l}$  can be expressed

by quantum defects  $\delta_{n,l}$  via

$$E_{n,l} = E_g - \frac{E_{\text{Ryd}}}{(n - \delta_{n,l})^2}, \quad (26)$$

with the excitonic Rydberg energy  $E_{\text{Ryd}}$ . The spherical symmetric semiclassical model, of course, does not provide the  $l$  splitting of the  $E_{n,l}$  levels in the crystal, however, they can be compared with the mean energies of the exact quantum mechanical  $l$  manifolds, when weighting each level by its multiplicity.

For our semiclassical calculations we use the spherically symmetric energy surface (21) with  $\Delta = 131$  meV and  $\mu' = 0.47$  to allow for direct comparisons with the results in Ref. [39]. The quantum defects  $\delta_{n,l}$  up to  $n = 25$  for  $s$ ,  $p$ ,  $d$ , and  $f$  states are shown in Fig. 2(a). It can be seen that the quantum defects are positive and increase and saturate with increasing  $n$ , while for increasing  $l$  the quantum defects decrease as expected.

The quantum defects obtained within the semiclassical picture are accurate enough to reproduce the measured energies in Ref. [39] up to meV precision. In Refs. [37, 38] experimental spectra have been compared with an improved spherical model obtained by using a weighted average of the band structure with cubic symmetry along the [100] and [111] directions, where analytical expressions are known. A comparison of these results with the quantum defects in Fig. 2(a) unveils that the semiclassical quantum defects are overestimated in the simple spherical model for higher angular momentum quantum numbers. A possible reason is that the fit to the spherical average was performed up to the maximum allowed value of the momentum in a hydrogen-like  $s$  state. As can be seen from Eq. (22) the classically allowed momentum range decreases for increasing  $l$ . The determination of the parameter  $\mu'$  can be improved by considering the probability distribution of the exciton in momentum space. Since the energy surfaces only play a role in the quantization for the radial direction, we assume a WKB wave function  $\psi_r \sim |p_r|^{-1/2} \exp(iS_r/\hbar)$  in this direction, which leads to the approximate probability distribution

$$|\psi_r|^2 \sim |p_r|^{-1} = \left[ p^2 - \left( l + \frac{1}{2} \right)^2 p^4/4 \right]^{-1/2}. \quad (27)$$

When the fitting procedure is adapted to the corresponding momentum range and probability distribution, this in fact leads to improved values  $\mu'_l$  for different angular quantum numbers  $l$ . We obtain  $\mu'_s = 0.51$ ,  $\mu'_p = 0.40$ ,  $\mu'_d = 0.37$ , and  $\mu'_f = 0.34$ . Each value can be understood as an order parameter characterizing the exciton dynamics on a specific  $l$  manifold. For increasing  $l$  the spherical corrections become less important leading to a more dominant hydrogen-like behavior. Repeating the quantization procedure for the different models provides the quantum defects shown in Fig. 2(b). The  $\delta_{n,l}$  are now slightly increased for  $l = 0$  but shifted downwards for  $l \geq 1$ . This provides a good agreement of semiclassical and quantum mechanical values, where the quantum defects for large  $n$  saturate to  $\delta_s = 0.65$ ,  $\delta_p = 0.34$ ,  $\delta_d = 0.18$ , and  $\delta_f = 0.12$  [49], marked by the solid lines in Fig. 2(b). In the semiclassical framework we find  $\delta_s = 0.63$ ,

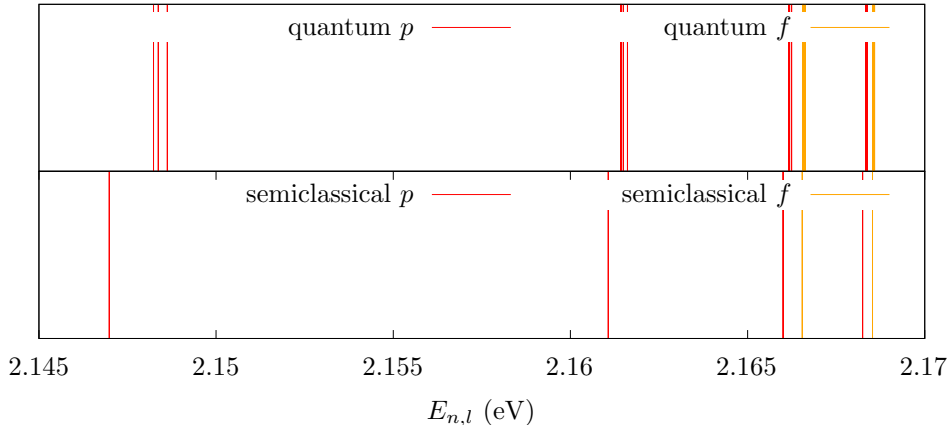


**Fig. 3** Comparison of energies  $E_{n,l}$  of odd parity states with  $n = 2$  to  $5$  obtained by numerically exact quantum calculations (top) with the semiclassical model using order parameters (bottom).

$\delta_p = 0.29$ ,  $\delta_d = 0.15$ , and  $\delta_f = 0.09$ , providing a good agreement with the literature values. In fact the semiclassical results are closer to the quantum mechanical results and experimental findings in Refs. [37, 38] than some values obtained by perturbative approaches [49].

Finally, we compare our semiclassical results with numerically exact eigenvalues of the Hamiltonian (6) obtained by the method introduced in Ref. [23]. We restrict the comparison to odd-parity states with  $n = 2$  to  $5$ , which are not affected by central-cell corrections [25] and a coupling to the green  $1s$  exciton [50, 51]. The  $l$  manifolds obtained via exact diagonalization are presented in the top of Fig. 3. The splitting of different  $l$  manifolds cannot be described within our spherical model. However, the levels obtained by the semiclassical model (bottom) show a good agreement with the groups for  $p$  and  $f$  manifolds of the numerically exact results. The semiclassically obtained energies lie systematically below the numerically exact eigenvalues and approach the quantum results for increasing principal quantum number  $n$  and angular momentum quantum number  $l$  as expected. Note that our spherical model with order parameters outperforms the spherical models introduced previously in the literature [37–39], for which the quantum defects were even bigger than our results and thus further away from numerically exact calculations.

## 4 Conclusion and outlook

In this article we developed and applied a spherically symmetric semiclassical model for the description of excitons in cuprous oxide. Therefore we used an adiabatic approach to calculate the energy surfaces corresponding to the yellow exciton series by diagonalization of the band-structure Hamiltonian in a basis for the quasispin and hole spin degrees of freedom, while treating the components of the momentum  $\mathbf{p}$  as classical parameters. Exploiting Kramers' theorem we could derive analytical formulas for the

energy surfaces with a cubic  $O_h$  symmetry. The exact band structure of semiconductors such as cuprous oxide can be computed, e.g., by application of density functional theory (DFT) [52]. Since our energy surfaces are equivalent to the band structure, the derived analytical formulas can be used for fitting the Luttinger parameters of the Suzuki-Hensel Hamiltonian to match spin-DFT calculations.

Spherically symmetric energy surfaces have been obtained by numerical averaging of all orientations of the momenta, and have been fitted with few parameters to analytical functions. The different  $l$  manifolds can be characterized by order parameters describing the strength of the band structure contributions. They are the basis for an EBK quantization to obtain semiclassical energy eigenvalues and quantum defects. The results have been compared with earlier spherical models [37–39] and exact quantum computations for  $\text{Cu}_2\text{O}$ . The same procedure can in principle also be applied to other semiconductors with different symmetries.

The spherically symmetric model does not provide the energy splittings of  $(n, l)$  manifolds. While the existence of a classical exciton dynamics has already been demonstrated by using energy surfaces with the full cubic symmetry [34, 35] a direct semiclassical calculation of the energy levels is still missing. In the future it will therefore be interesting to see whether the semiclassical quantization scheme can be extended to correctly reproduce the fine-structure splittings of the yellow exciton series in cuprous oxide. Furthermore, the analytical expressions for the energy surfaces may be used to describe the spectra of magnetoexcitons in regions where quantum mechanical calculations are no longer feasible [53]. To this end the closed-orbit theory developed by Du and Delos [54, 55] may be adopted using energy surfaces to describe the photoabsorption spectra of magnetoexcitons near the ionization threshold.

**Acknowledgements.** This work was supported by Deutsche Forschungsgemeinschaft (DFG) through Grants No. MA1639/16-1 and No. PF381/18-2 under DFG SPP1929 “Giant interactions in Rydberg systems (GiRyd).”

**Data availability.** The data that support the findings of this study are available from the corresponding author upon reasonable request.

## References

- [1] Balmer, J.J.: Notiz über die Spectrallinien des Wasserstoffs. *Annalen der Physik* **261**, 80–87 (1885) <https://doi.org/10.1002/andp.18852610506>
- [2] Rydberg, J.R.: On the structure of the line-spectra of the chemical elements. The London, Edinburgh, and Dublin Philosophical Magazine and Journal of Science **29**, 331–337 (1890) <https://doi.org/10.1080/14786449008619945>
- [3] Lyman, T.: The spectrum of hydrogen in the region of extremely short wavelengths. *Astrophysical Journal* **23**, 181 (1906) <https://doi.org/10.1086/141330>
- [4] Paschen, F.: Zur Kenntnis ultraroter Linienspektren. I. (Normalwellenlängen bis 27000 Å.-E.). *Annalen der Physik* **332**, 537–570 (1908) <https://doi.org/10.1002/andp.19083321303>

- [5] Bohr, N.: I. On the constitution of atoms and molecules. The London, Edinburgh, and Dublin Philosophical Magazine and Journal of Science **26**, 1–25 (1913) <https://doi.org/10.1080/14786441308634955>
- [6] Sommerfeld, A.: Zur Quantentheorie der Spektrallinien. Annalen der Physik **356**, 1–94 (1916) <https://doi.org/10.1002/andp.19163561702>
- [7] Einstein, A.: Zum Quantensatz von Sommerfeld und Epstein. Verh. d. D. Physik. Ges., 82–92 (1917)
- [8] Brillouin, L.: Remarques sur la mécanique ondulatoire. J. Phys. Radium **7**, 353–368 (1926) <https://doi.org/10.1051/jphysrad:01926007012035300>
- [9] Keller, J.B.: Corrected Bohr-Sommerfeld quantum conditions for nonseparable systems. Annals of Physics **4**, 180–188 (1958) [https://doi.org/10.1016/0003-4916\(58\)90032-0](https://doi.org/10.1016/0003-4916(58)90032-0)
- [10] Maslov, V.P., Fedoriuk, M.V.: Semi-classical Approximation in Quantum Mechanics. Springer, Berlin (2001)
- [11] Gutzwiller, M.C.: Phase-Integral Approximation in Momentum Space and the Bound States of an Atom. Journal of Mathematical Physics **8**, 1979–2000 (1967) <https://doi.org/10.1063/1.1705112>
- [12] Gutzwiller, M.C.: Periodic Orbits and Classical Quantization Conditions. Journal of Mathematical Physics **12**, 343–358 (1971) <https://doi.org/10.1063/1.1665596>
- [13] Gutzwiller, M.C.: Chaos in Classical and Quantum Mechanics. Springer, New York (1990). <https://doi.org/10.1007/978-1-4612-0983-6>
- [14] Brack, M., Bhaduri, R.: Semiclassical Physics. Addison-Wesley Publishing, Reading (1997)
- [15] Baldini, G.: Ultraviolet absorption of solid argon, krypton, and xenon. Phys. Rev. **128**, 1562–1567 (1962) <https://doi.org/10.1103/PhysRev.128.1562>
- [16] Sturge, M.D.: Optical absorption of gallium arsenide between 0.6 and 2.75 eV. Phys. Rev. **127**, 768–773 (1962) <https://doi.org/10.1103/PhysRev.127.768>
- [17] Mueller, T., Malic, E.: Exciton physics and device application of two-dimensional transition metal dichalcogenide semiconductors. npj 2D Materials and Applications **2**, 29 (2018) <https://doi.org/10.1038/s41699-018-0074-2>
- [18] Gross, E.F.: Optical spectrum of excitons in the crystal lattice. Il Nuovo Cimento (1955-1965) **3**, 672–701 (1956) <https://doi.org/10.1007/BF02746069>
- [19] T. Kazimierczuk, D. Fröhlich, S. Scheel, H. Stolz, M. Bayer: Giant Rydberg excitons in the copper oxide Cu<sub>2</sub>O. Nature **514**, 343–347 (2014) <https://doi.org/10.1038/nature13000>

- [20] Versteegh, M.A., Steinhauer, S., Bajo, J., Lettner, T., Soro, A., Romanova, A., Gyger, S., Schweickert, L., Mysyrowicz, A., Zwiller, V.: Giant Rydberg excitons in  $\text{Cu}_2\text{O}$  probed by photoluminescence excitation spectroscopy. *Phys. Rev. B* **104**, 245206 (2021) <https://doi.org/10.1103/PhysRevB.104.245206>
- [21] Luttinger, J.M., Kohn, W.: Motion of electrons and holes in perturbed periodic fields. *Phys. Rev.* **97**, 869–883 (1955) <https://doi.org/10.1103/PhysRev.97.869>
- [22] Luttinger, J.M.: Quantum theory of cyclotron resonance in semiconductors: General theory. *Phys. Rev.* **102**, 1030–1041 (1956) <https://doi.org/10.1103/PhysRev.102.1030>
- [23] Schweiner, F., Main, J., Feldmaier, M., Wunner, G., Uihlein, C.: Impact of the valence band structure of  $\text{Cu}_2\text{O}$  on excitonic spectra. *Phys. Rev. B* **93**, 195203 (2016) <https://doi.org/10.1103/PhysRevB.93.195203>
- [24] Koster, G.F., Dimmock, J.O., Wheeler, R.G., Statz, H.: Properties of the Thirty-two Point Groups. Massachusetts Institute of Technology Press research monograph. M.I.T. Press, Cambridge (1963). <https://books.google.de/books?id=iMTQAAAAMAAJ>
- [25] Schweiner, F., Main, J., Wunner, G., Uihlein, C.: Even exciton series in  $\text{Cu}_2\text{O}$ . *Phys. Rev. B* **95**, 195201 (2017) <https://doi.org/10.1103/PhysRevB.95.195201>
- [26] Haken, H.: Die Theorie des Exzitons im festen Körper. *Fortschritte der Physik* **6**, 271–334 (1958) <https://doi.org/10.1002/prop.19580060602>
- [27] Haken, H.: Zur Quantentheorie des Mehrelektronensystems im schwingenden Gitter. Teil 1. *Zeitschrift für Physik* **146**, 527 (1956)
- [28] Haken, H.: Kopplung nichtrelativistischer Teilchen mit einem quantisierten Feld. Teil 1. Das Exziton im schwingenden, polaren Kristall. *Il Nuovo Cimento* (1955–1965) **3**, 1230 (1956) <https://doi.org/10.1007/BF02785005>
- [29] Haken, H.: Der heutige Stand der Exzitonenforschung in Halbleitern, pp. 1–48. Springer, Berlin, Heidelberg (1957). <https://doi.org/10.1007/BFb0119037>
- [30] Haken, H., Schottky, W.: Die Behandlung des Exzitons nach der Vielelektronentheorie. *Zeitschrift für Physikalische Chemie* **16**, 218–244 (1958) <https://doi.org/10.1524/zpch.1958.16.3.6.218>
- [31] Kuper, C.G., Whitfield, G.D.G.D.: Polarons and Excitons. Edited by C. G. Kuper and G. D. Whitfield. Plenum Press, New York (1963). Scottish Universities Summer School in Physics (3rd : 1962 : St. Andrews, Scot.)
- [32] Ertl, J., Rommel, P., Mom, M., Main, J., Bayer, M.: Classical and semiclassical



- description of Rydberg excitons in cuprous oxide. *Phys. Rev. B* **101**, 241201 (2020) <https://doi.org/10.1103/PhysRevB.101.241201>
- [33] Ertl, J., Rentschler, S., Main, J.: Rydberg excitons in cuprous oxide: A two-particle system with classical chaos. *Chaos: An Interdisciplinary Journal of Nonlinear Science* **34**, 103104 (2024) <https://doi.org/10.1063/5.0210792>
- [34] Ertl, J., Marquardt, M., Schumacher, M., Rommel, P., Main, J., Bayer, M.: Signatures of exciton orbits in quantum mechanical recurrence spectra of  $\text{Cu}_2\text{O}$ . *Phys. Rev. Lett.* **129**, 067401 (2022) <https://doi.org/10.1103/PhysRevLett.129.067401>
- [35] Ertl, J., Marquardt, M., Schumacher, M., Rommel, P., Main, J., Bayer, M.: Classical dynamics and semiclassical analysis of excitons in cuprous oxide. *Phys. Rev. B* **109**, 165203 (2024) <https://doi.org/10.1103/PhysRevB.109.165203>
- [36] Heckötter, J., Farenbruch, A., Fröhlich, D., Afmann, M., Yakovlev, D.R., Bayer, M., Semina, M.A., Glazov, M.M., Rommel, P., Ertl, J., Main, J., Stolz, H.: The energy level spectrum of the yellow excitons in cuprous oxide. *Physics Reports* **1100**, 1–69 (2025) <https://doi.org/10.1016/j.physrep.2024.10.004>
- [37] Schöne, F., Krüger, S.-O., Grünwald, P., Afmann, M., Heckötter, J., Thewes, J., Stolz, H., Fröhlich, D., Bayer, M., Scheel, S.: Coupled valence band dispersions and the quantum defect of excitons in  $\text{Cu}_2\text{O}$ . *Journal of Physics B: Atomic, Molecular and Optical Physics* **49**, 134003 (2016) <https://doi.org/10.1088/0953-4075/49/13/134003>
- [38] Schöne, F., Krüger, S.-O., Grünwald, P., Stolz, H., Scheel, S., Afmann, M., Heckötter, J., Thewes, J., Fröhlich, D., Bayer, M.: Deviations of the exciton level spectrum in  $\text{Cu}_2\text{O}$  from the hydrogen series. *Phys. Rev. B* **93**, 075203 (2016) <https://doi.org/10.1103/PhysRevB.93.075203>
- [39] Uihlein, C., Fröhlich, D., Kenklies, R.: Investigation of exciton fine structure in  $\text{Cu}_2\text{O}$ . *Phys. Rev. B* **23**, 2731–2740 (1981) <https://doi.org/10.1103/PhysRevB.23.2731>
- [40] Lipari, N.O., Altarelli, M.: Theory of indirect excitons in semiconductors. *Phys. Rev. B* **15**, 4883–4897 (1977) <https://doi.org/10.1103/PhysRevB.15.4883>
- [41] Baldereschi, A., Lipari, N.O.: Spherical model of shallow acceptor states in semiconductors. *Phys. Rev. B* **8**, 2697–2709 (1973) <https://doi.org/10.1103/PhysRevB.8.2697>
- [42] Edmonds, A.R.: *Angular Momentum in Quantum Mechanics. Investigations in physics.* Princeton University Press, Princeton (1996). <https://doi.org/10.1515/9781400884186> . <https://books.google.de/books?id=0BSOg0oHhZ0C>
- [43] Broeckx, J.: Acceptor excitation spectra in germanium in a uniform magnetic

- field. Phys. Rev. B **43**, 9643–9648 (1991) <https://doi.org/10.1103/PhysRevB.43.9643>
- [44] Anderson, E., Bai, Z., Bischof, C., Blackford, S., Demmel, J., Dongarra, J., Croz, J.D., Greenbaum, A., Hammarling, S., McKenney, A.: LAPACK Users' Guide, Third Edition. Society for Industrial and Applied Mathematics, Philadelphia (1999)
- [45] Kramers, H.: General theory of paramagnetic rotation in crystals. In: Proc. Acad. Sci. Amsterdam, vol. 33, p. 959 (1930)
- [46] Schöne, F.: Optical properties of yellow excitons in cuprous oxide. PhD thesis, Universität Rostock (2017)
- [47] Bewersdorff, J.: Algebra für Einsteiger. Springer, Wiesbaden (2019). <https://doi.org/10.1007/978-3-658-26152-8>
- [48] Womersley, R.S.: Efficient spherical designs with good geometric properties. In: Dick, J., Kuo, F.Y., Woźniakowski, H. (eds.) Contemporary Computational mathematics—A Celebration of the 80th Birthday of Ian Sloan, pp. 1243–1285. Springer, Cham (2018)
- [49] Heckötter, J., Freitag, M., Fröhlich, D., Aßmann, M., Bayer, M., Semina, M., Glazov, M.: Scaling laws of Rydberg excitons. Phys. Rev. B **96**, 125142 (2017) <https://doi.org/10.1103/PhysRevB.96.125142>
- [50] Rommel, P., Main, J., Farenbruch, A., Yakovlev, D.R., Bayer, M.: Exchange interaction in the yellow exciton series of cuprous oxide. Phys. Rev. B **103**, 075202 (2021) <https://doi.org/10.1103/PhysRevB.103.075202>
- [51] Heckötter, J., Rommel, P., Main, J., Aßmann, M., Bayer, M.: Analysis of the fine structure of the D-exciton shell in cuprous oxide. physica status solidi (RRL) – Rapid Research Letters (2021) <https://doi.org/10.1002/pssr.202100335>
- [52] French, M., Schwartz, R., Stolz, H., Redmer, R.: Electronic band structure of Cu<sub>2</sub>O by spin density functional theory. Journal of Physics: Condensed Matter **21**, 015502 (2008) <https://doi.org/10.1088/0953-8984/21/1/015502>
- [53] Schweiner, F., Main, J., Wunner, G., Freitag, M., Heckötter, J., Uihlein, C., Aßmann, M., Fröhlich, D., Bayer, M.: Magnetoexcitons in cuprous oxide. Phys. Rev. B **95**, 035202 (2017) <https://doi.org/10.1103/PhysRevB.95.035202>
- [54] L. Du, M., B. Delos, J.: Effect of closed classical orbits on quantum spectra: Ionization of atoms in a magnetic field. I. Physical picture and calculations. Phys. Rev. A **38**, 1896–1912 (1988) <https://doi.org/10.1103/PhysRevA.38.1896>

- [55] Du, M.L., Delos, J.B.: Effect of closed classical orbits on quantum spectra: Ionization of atoms in a magnetic field. II. Derivation of formulas. *Phys. Rev. A* **38**, 1913–1930 (1988) <https://doi.org/10.1103/PhysRevA.38.1913>